JGR Atmospheres

RESEARCH ARTICLE
10.1029/2023JD040084

Key Points:

- We set up an automated system to monitor rain and vapor isotopes continuously and simultaneously over 324 rain events from 2016 to 2019
- Rain and vapor isotope values deviated from equilibrium during most of the rain events
- Below cloud rain-vapor interactions significantly modulate the evolution of rain and vapor isotopes during individual rain events

Supporting Information:

Supporting Information may be found in the online version of this article.

Correspondence to:

S. He,
snhe@ntu.edu.sg;
heshaoneng@gmail.com

Citation:

He, S., Jackisch, D., Feng, L., Samanta, D., Wang, X., & Goodkin, N. F. (2024). Uncovering below cloud rain-vapor interactions during tropical rain events through simultaneous and continuous real-time monitoring of rain and vapor isotopes. *Journal of Geophysical Research: Atmospheres*, *129*, e2023JD040084. https://doi.org/10.1029/2023JD040084

Received 27 SEP 2023
Accepted 3 NOV 2024

Uncovering Below Cloud Rain-Vapor Interactions During Tropical Rain Events Through Simultaneous and Continuous Real-Time Monitoring of Rain and Vapor Isotopes

Shaoneng He[1], Dominik Jackisch[1], Lujia Feng[1,2], Dhrubajyoti Samanta[1], Xianfeng Wang[1,2], and Nathalie F. Goodkin[3]

[1]Earth Observatory of Singapore, Nanyang Technological University, Singapore, Singapore, [2]Asian School of the Environment, Nanyang Technological University, Singapore, Singapore, [3]Division of Physical Sciences, American Museum of Natural History, New York, NY, USA

Abstract Due to limited water vapor measurements, vapor isotopes have been traditionally estimated under the assumption of isotopic equilibrium between rain and vapor below cloud base. However, recent advancements in analytical instruments allow more vapor isotopic measurements that have challenged this assumption. To enhance our understanding of rain-vapor interactions below cloud base in tropical regions, we established an automated system to measure rain and vapor isotopes simultaneously and continuously in real time at minute intervals in Singapore. Among 324 rain events monitored from 2016 to 2019, 81% exhibited a substantial departure of rain and vapor isotopes from the expected equilibrium. This departure suggests that raindrop evaporation plays a larger role in determining their isotopes. The conclusion is supported by the generally lower slopes of the local meteoric water line. Seasonal variations in rain event characteristics indicate changing influences of rain-vapor interactions: during monsoons, more frequent heavy rainfall maintains relatively high humidity below cloud base, favoring rain-vapor isotopic equilibrium, whereas during inter-monsoons, more light rain events lead to pronounced rain evaporation and larger isotopic differences. Furthermore, rain-vapor interactions below cloud base significantly modulated their isotope evolution during individual events. As events progressed, reduced humidity favored evaporation, increasing rain isotope values and decreasing its d-excess, whereas vapor isotope values decreased and its d-excess increased. Our study introduces a new approach to capturing real-time high-resolution rain and vapor isotopes at minute intervals to understand the dynamics of rain-vapor interactions below cloud base. Findings underscore the crucial role of these interactions in influencing rain and vapor isotopes during tropical rain events.

Plain Language Summary In this research, we investigated how rain and water vapor interact beneath clouds in tropical areas. Traditionally, scientists assumed that rain and vapor isotopes are in equilibrium, but recent vapor measurements have challenged this notion. To delve deeper, we set up an automated system to continuously and simultaneously measure rain and vapor isotopes at minute intervals in Singapore. We monitored 324 rain events from 2016 to 2019 and discovered that for most events, rain and vapor isotopes deviated from the expected equilibrium. This suggests that the raindrops often evaporate significantly before hitting the ground, altering both rain and vapor isotopes and influencing their isotopic evolution during these events. For example, reduced humidity with a low rain rate and small raindrops toward an event's end promoted more evaporation, causing rain and vapor to move even further from isotopic equilibrium. In conclusion, this study highlights the significant role of below-cloud processes in shaping rain and vapor isotopes during tropical rain events. This knowledge can assist scientists in better comprehending these intricate processes, which are typically challenging to measure accurately.

1. Introduction

Water isotopologues, namely, $H_2{}^{16}O$, $H_2{}^{18}O$, and $HD^{16}O$, are distributed differentially in different phases (solid, liquid, and vapor) through kinetic and equilibrium fractionations. Water stable isotopes ($\delta^{18}O$, $\delta^{2}H$, and d-excess), therefore, record physical conditions during these processes and have been used as natural tracers to study climate and hydrological processes (Dee et al., 2023). Examination of global precipitation isotopes reveals the relationships between precipitation isotopes and climate, specifically the temperature effect at the middle- to

high-latitudes and the amount effect at the low latitudes (Dansgaard, 1964; Rozanski et al., 1993; Schotterer et al., 1996). These relationships have found application in paleoclimate studies, such as using ice cores to reconstruct past temperature (e.g., Jouzel, 2003; Klein et al., 2016) and speleothems to uncover monsoon histories (e.g., Liu et al., 2020; Wang et al., 2017; Wong et al., 2021). Observations in the tropics indicate that regionally organized convective activities have more influence on precipitation isotopes than the local amount effect (He, Goodkin, Jackisch, et al., 2018, He, Goodkin, Kurita, et al., 2018; He et al., 2021; Kurita, 2013; Lekshmy et al., 2014; Moerman et al., 2013; Nlend et al., 2020; Zwart et al., 2016), and cloud microphysics also affect rain isotopes (He, Goodkin, Kurita, et al., 2018; Muller et al., 2014; Munksgaard et al., 2019; Risi et al., 2010). Knowledge gained by investigating water isotopes provides validation for climate models that predict Earth's future climate (Field et al., 2014; Lee et al., 2009; Nusbaumer et al., 2017; Ramos et al., 2022).

However, for many years, studies of water isotopes have largely focused on precipitation (rain and snow) with much fewer investigations conducted on vapor isotopes (Wei et al., 2019) despite water vapor being a key component of the hydrological cycle. This can be attributed to the challenge of obtaining vapor samples for isotope analysis using the traditional method, that is, cryogenic trapping (Casado et al., 2016; Deshpande et al., 2010; Fiorella et al., 2018; Galewsky et al., 2011, 2016; Rahul et al., 2016; Tian et al., 2020; Wei et al., 2019). With the advancement in analytical instruments, in particular, the availability of relatively low-cost laser absorption spectrometers, the recent couple of decades have seen more investigations of vapor isotopes (e.g., Galewsky et al., 2016; Wei et al., 2019). These investigations have significantly enriched our knowledge of the mechanisms underlying hydrological processes, such as moisture sources and their transport pathways, evapotranspiration, evaporation processes, moisture recycling, and convection processes (Aemisegger et al., 2015; Angert et al., 2008; Benetti et al., 2018; Bhattacharya et al., 2022; Bonne et al., 2019; Casado et al., 2016; Conroy et al., 2016; Dai et al., 2021; Fiorella et al., 2018; Galewsky et al., 2016; González et al., 2016; Good et al., 2015; Lekshmy et al., 2018; Noone, 2012; Noone et al., 2013; Samuels-Crow et al., 2014; Sinha & Chakraborty, 2020; Tian et al., 2020). Compared to other regions, measurements of vapor isotopes in low latitudes, specifically tropical regions, are limited (e.g., Wei et al., 2019). Therefore, investigating isotopes of vapor in tropical regions, the primary source of precipitation, can bridge the existing knowledge gap, providing valuable insights into the isotopic composition of vapor in these important climatic zones.

When falling through the air below cloud base, raindrops continuously exchange their water molecules with the surrounding vapor, and thermodynamics drive the exchange toward isotope equilibrium. Under unsaturated conditions, raindrops will undergo partial evaporation below cloud base, causing nonequilibrium or kinetic isotope fractionation. Accurate representation of this process is very important for climate models as the process impacts precipitation characteristics and the dynamics of climate systems (Graf et al., 2019). Because of the lack of vapor measurements, vapor isotope values were calculated based on isotopic equilibrium between rain and vapor below cloud base (Fiorella et al., 2019; Gat, 1996; Gibson et al., 2008; Jasechko et al., 2013). However, recent high-resolution simultaneous measurements of rain and vapor isotopes (e.g., Graf et al., 2019; Mercer et al., 2020; Vimeux & Risi, 2021) suggest that such an assumption may not hold true. Fiorella et al. (2019) also assessed this assumption using simulations from eight climate models and found that modeled atmospheric vapor has less negative isotope value than the vapor in equilibrium with annual precipitation. Further, the deviation from equilibrium generally increases from low latitudes to high latitudes. More observations, specifically simultaneous measurements of both rain and vapor isotopes, are necessary to improve our understanding of the interaction between raindrops and vapor below cloud base and validate the model simulations. Although rain-vapor interaction has been a topic of recent observations (e.g., Graf et al., 2019; Mercer et al., 2020; Vimeux & Risi, 2021), these studies either have short observation durations or focus primarily on higher latitude regions. More importantly, the sampling resolutions for rain and vapor during these observations are not equivalent, as rain samples were not analyzed continuously in real time together with vapor.

In this study, we used a custom-built automated system equipped with laser absorption spectrometers to measure in situ isotopes of rain and vapor simultaneously and continuously at minute intervals in Singapore, a unique approach that had never been used before. Our primary objective was to investigate the interactions between raindrops and water vapor below cloud base during tropical rain events. To achieve this, we examined a total of 324 rain events from Dec-2016 to Mar-2019 in our investigation. Additionally, we explored what controls the long-term evolution of rain and vapor isotopes at a longer timescale over the study period.

2. Materials and Methods

2.1. Sampling Site Description

The measurement of rainwater and vapor isotopes was conducted in our geochemistry laboratory (1.35°N, 103.68°E, altitude 40 m above sea level) inside the building that hosts the Earth Observatory of Singapore (EOS) and the Asian School of the Environment (ASE), Nanyang Technological University (NTU), Singapore. The NTU main campus is situated in the south-western part of Singapore, an island city-state located at the end of the Malayan Peninsula (Figure S1 in Supporting Information S1).

Near the equator, Singapore exhibits a typical tropical climate characterized by abundant rainfall, warm temperature, and high humidity throughout the year. Its climate is distinguished by two alternating monsoon seasons, the northeast (NE) and southwest (SW) monsoon, separated by two inter-monsoon periods (Figure S1 in Supporting Information S1). The NE monsoon occurs between December and March with dominant northerly to northeasterly winds, whereas the SW monsoon occurs between June and September with prevalent southeasterly to southerly winds. During the April–May and October–November inter-monsoons, winds are generally light and variable in direction. During the NE monsoon, the presence of a high-pressure system over Siberia frequently triggers cold surges, resulting in prolonged periods of continuous and widespread rain in the region. Another major weather system that affects Singapore and brings heavy rainfall is the Sumatra Squall, an organized line of thunderstorms extending for hundreds of kilometers and traveling across Singapore (He, Goodkin, Jackisch, et al., 2018; He, Goodkin, Kurita, et al., 2018). Primarily observed in the SW monsoon, the Sumatra Squalls often occur in the early morning and originate over Sumatra or the Straits of Malacca.

2.2. Instrument Configuration and Isotope Analysis

Figure 1 demonstrates the major components of our automated system for isotope analysis of rain and vapor; with this system, we obtained in situ stable isotope compositions of both rain and vapor continuously and in real time at minute intervals without the need for actual sample collection. The module for rainwater consists of a rain panel, a carboy for reference water, a floating switch, a peristaltic pump, and a diffusion sampler coupled to a Picarro L2130-i (DS-CRDS). The top of the rain panel is a 2 m^2 nonadhesive polypropylene plastic sheet with a semicircular pipe attached at its low end, which allows sufficient rainwater to quickly drain through 1/4-inch plastic tubing to a collection vessel inside the lab with a floating switch connected to a two-way pinch valve. Holes on the side of the semicircular pipe with the collection panel and on the side of the collection vessel facilitate rainwater drainage, preventing overflow during heavy rainfall events. When there is no rain, the pump delivers the reference water with known isotope values in the carboy to the DS-CRDS (more details in Text S1). During a rain event, the floating switch will trigger the pinch valve to switch to rainwater, which will be delivered by the pump to the DS. Inside the DS, there is an inner chamber with a semipermeable expanded Teflon (ePTFE) tubing that permits water vapor to diffuse across the ePTFE tubing into the chamber, and then vapor will be introduced directly into the CRDS for isotope analysis (Munksgaard et al., 2011; Figure 2 in He, Goodkin, Jackisch, et al., 2018). To cope with the accumulation of fine particles that typically adhere to the inside walls of the tubing in the system, we routinely replaced all the tubing every two to 3 months. Meanwhile, we cleaned the rain collection panel and collection vessel to remove the dust deposits on their surfaces. The DS-CRDS continuously recorded measurements every second, and we reported integrated data over 1-min intervals. The DS-CRDS system was calibrated on the day when there was a rain event. For calibration, we used three in-house standards (KONA, ICELAND, and TIBET; Table S1 in Supporting Information S1) with $\delta^{18}O$ and $\delta^{2}H$ ranging from 0 to −20‰ and 0 to −144‰, respectively. Precision is 0.2‰ or better for $\delta^{18}O$ and 0.4‰ for $\delta^{2}H$ based on long-term analysis of our quality assurance/quality control (QA/QC) standard.

The module for vapor includes a 1/8-inch copper tubing, a standard delivery module (SDM), a vapourizer, and a Picarro L2130-*i*. The copper tubing (∼6 m) is extended outside the building (at a height of ∼30 m above the ground) through which vapor was pumped continuously at 0.6 L/min using a diaphragm pump and introduced to the Picarro L130-*i* through the vapourizer for isotope analysis. To prevent the condensation of vapor, the tubing was wrapped with heating tape with the temperature maintained at 60°C. The SDM delivered our two water vapor isotope standards (KONA and MixW; Table S1 in Supporting Information S1) to the analyzer via the vapourizer for calibration, and the system was calibrated every 24 hr. Since the measured isotope values tend to change with water vapor volume mixing ratios, known as size fractionation, it is necessary to correct the data for this effect.

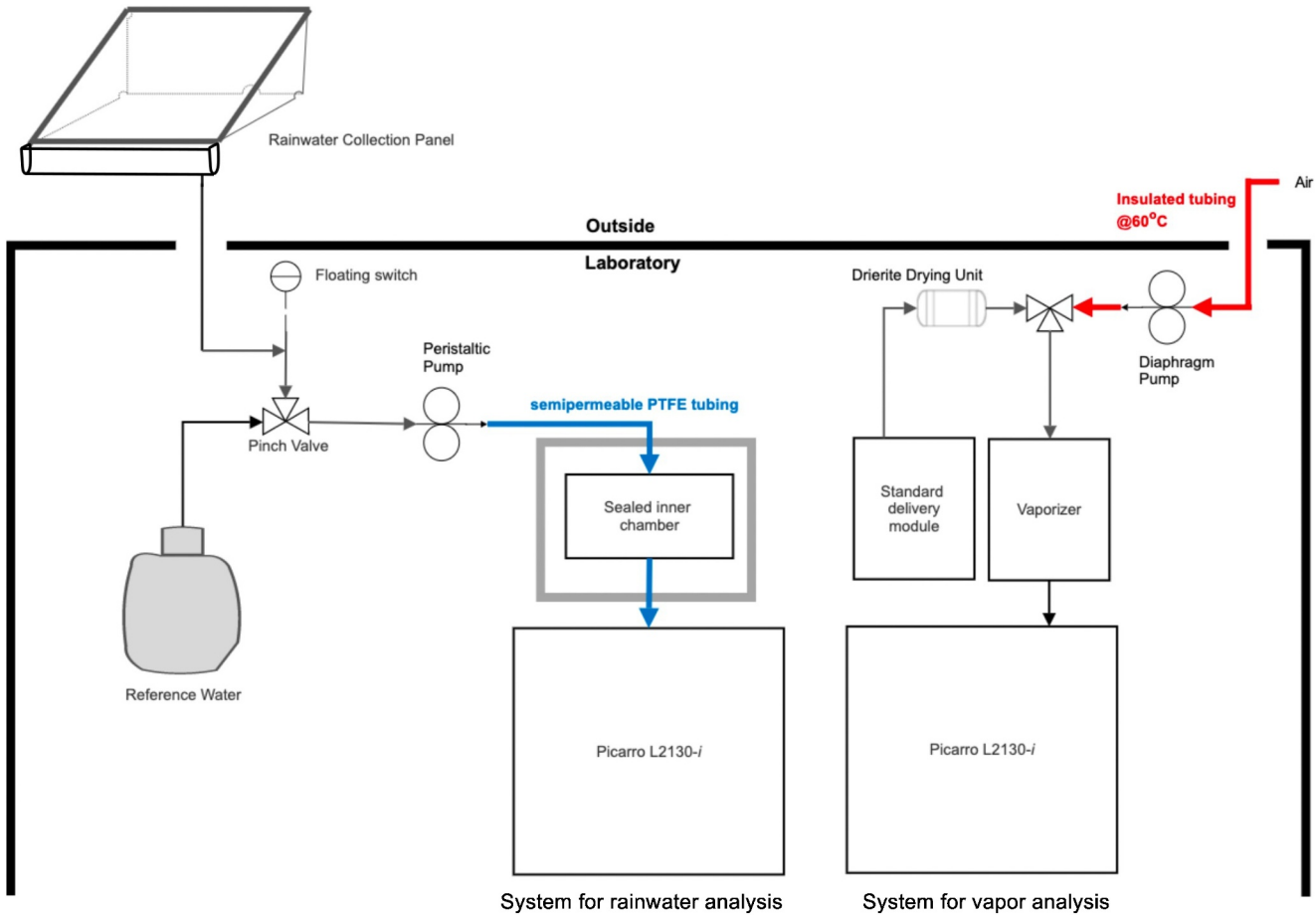

Figure 1. A schematic for the automated system to measure in situ stable isotopes of rain and vapor simultaneously and continuously without collecting discreet samples.

Through the software control, one standard with different volumes was analyzed and the linear correlation established between the isotope values and water vapor mixing ratios was used for the correction.

2.3. Meteorological Data

On-site temperature (T), relative humidity (RH), and rainfall amount were obtained from our HOBO Data Logging Rain Gauge installed on the rooftop of our lab building. Regional rainfall data between 1978 and 2022 were taken from MSWEP, a global precipitation product with a 3-hourly 0.1 resolution (http://www.gloh2o.org/mswep/). The product merges gauge, satellite, and reanalysis data to obtain the highest-quality precipitation estimates. Outgoing longwave radiation (OLR) data was accessed from NOAA with a horizontal resolution of $1° \times 1°$ (https://www.ncdc.noaa.gov/cdr/atmospheric).

2.4. Apparent Disequilibrium (Δδ)

The stable isotope values of water vapor deviate from the expected equilibrium values with rainwater when kinetic fractionation happens or when vapor mixes with air masses with different isotope values. The difference (Δδ) between the isotope value of vapor in equilibrium with precipitation (δve) and the measured value of vapor (δv) is calculated using the following equation:

$$\Delta\delta = \delta ve - \delta v \quad (1)$$

$\Delta\delta^{18}O$, $\Delta\delta^{2}H$, and Δd in the following sections refer to the difference between vapor's equilibrium and measured $\delta^{18}O$ that between its equilibrium and measured $\delta^{2}H$ and that between its equilibrium and actual d-excess,

respectively. Vapor $\delta^{18}O$ and $\delta^{2}H$ in isotopic equilibrium with rainwater are estimated using the following equilibrium fractionation factors between liquid and vapor (Horita et al., 2008):

$$10^3 \ln^2\alpha = 52.612 - 76.248\left(10^3/T\right) + 24.844\left(10^6/T^2\right) \quad (2)$$

$$10^3 \ln^{18}\alpha = -2.0667\text{–}0.4156\left(10^3/T\right) + 1.137\left(10^6/T^2\right) \quad (3)$$

where T is the temperature in Kelvin, and $^{18}\alpha$ and $^{2}\alpha$ are equilibrium factors for oxygen and hydrogen isotopes, respectively.

The temperature (T_i) of a falling hydrometeor, that is, a raindrop, can be estimated using on-site meteorological parameters (Harder & Pomeroy, 2013):

$$T_i = T_a + (D/\lambda_t)\, L\left(\rho_{Ta} - \rho_{sat(Ti)}\right) \quad (4)$$

where T_a is the on-site air temperature, D is the diffusion rate of vapor in air ($m^2\ s^{-1}$), L is the latent heat of sublimation or vapourization ($J\ Kg^{-1}$), λ_t is the thermal conductivity of air ($J\ m^{-1}\ s^{-1}\ C^{-1}$), ρ_{Ta} is the water vapor density of the free atmosphere ($kg\ m^{-3}$), and $\rho_{sat(Ti)}$ is the saturated water vapor pressure density of the hydrometeor ($kg\ m^{-3}$). Our calculations indicate that the discrepancy between T_i and T_a is quite small during rain events below 0.5°C, making it no difference to use either in our study.

3. Results

3.1. $\delta^{18}O$, $\delta^{2}H$, and D-Excess in Vapor and Rain

The stable isotopes of both vapor and rain show substantial variations over the study period (Figure 2a). Vapor $\delta^{18}O$ ($\delta^{18}O_v$) ranges from −27.37 to −9.66‰ and $\delta^{2}H$ ($\delta^{2}H_v$) from −206.36 to −69.16‰, whereas rainwater $\delta^{18}O$ ($\delta^{18}O_p$) ranges from −19.97 to 1.60‰ and $\delta^{2}H$ ($\delta^{2}H_p$) from −119.79 to 14.15‰. Similarly, d-excess of vapor (d_v) and rain (d_p) also exhibit large variations; d_v ranges from −3.85 to 28.01‰ and d_p from −14.36 to 38.35‰. Seasonal variability of both rain and vapor isotopes is evident in the time series of monthly average isotopes (Figure S2 in Supporting Information S1); the low isotope values are generally observed around monsoon seasons. However, the seasonal variability of d_v and, particularly, d_p is not pronounced.

Linear correlation analysis (Figures S3 in Supporting Information S1) reveals varying degrees but generally weak correlations between vapor isotopes and on-site meteorological parameters at different timescales from minute to monthly. Vapor $\delta^{18}O$ demonstrates a weak positive correlation with on-site T with $r = 0.20$ ($p < 0.01$) at minute scale, $r = 0.33$ ($p < 0.0001$) at daily scale, and $r = 0.31$ ($p < 0.0001$) at monthly scale. However, it exhibits a negative correlation with RH ranging from weak at minute scale ($r = -0.20$, $p < 0.0001$) to fair at both daily ($r = -0.43$, $p < 0.0001$) and monthly ($r = -0.49$, $r < 0.0001$) scales. Only a very weak negative correlation is also found between vapor $\delta^{18}O$ and rainfall with $r = -0.21$ ($p < 0.0001$) at minute scale, $r = -0.22$ ($p < 0.0001$) at daily scale, and $r = -0.30$ ($p < 0.0001$) at monthly scale.

A similar correlation is observed between rain $\delta^{18}O$ and on-site meteorological parameters (Figure S4 in Supporting Information S1). Rain $\delta^{18}O$ exhibits a weak positive correlation with on-site T at minute scale ($r = 0.35$, $p < 0.0001$) but surprisingly not at daily ($r = 0.07$, $p < 0.0001$) and monthly ($r = 0.02$, $p < 0.0001$) scales. Like vapor $\delta^{18}O$, rain $\delta^{18}O$ shows a weak correlation with RH with $r = -0.32$ ($p < 0.01$) at minute scale, $r = -0.16$ ($p < 0.0001$) at daily scale, and $r = -0.35$ ($p < 0.0001$) at monthly. At minute and daily scales, no correlation is found between vapor $\delta^{18}O$ and rainfall, whereas a weak correlation is detected at monthly scale ($r = -0.35$, $p < 0.0001$).

3.2. Local Meteoric Water Line (LMWL) and Local Vapor Line (LVL)

Slopes and intercepts of the Local Meteoric Water Line (LMWL) (defined by $\delta^{18}O_p$ and $\delta^{2}H_p$) and Local Vapor Line (LVL) (defined by $\delta^{18}O_v$ and $\delta^{2}H_v$) change with the seasons (Figure 3). During the SW monsoon, the LMWL has a slope of 7.80 and an intercept of 10.40 (Equation 5) similar to that of the global meteoric water line (GMWL) defined as $\delta^{2}H_p = 8*\delta^{18}O_p + 10$ (Craig, 1961):

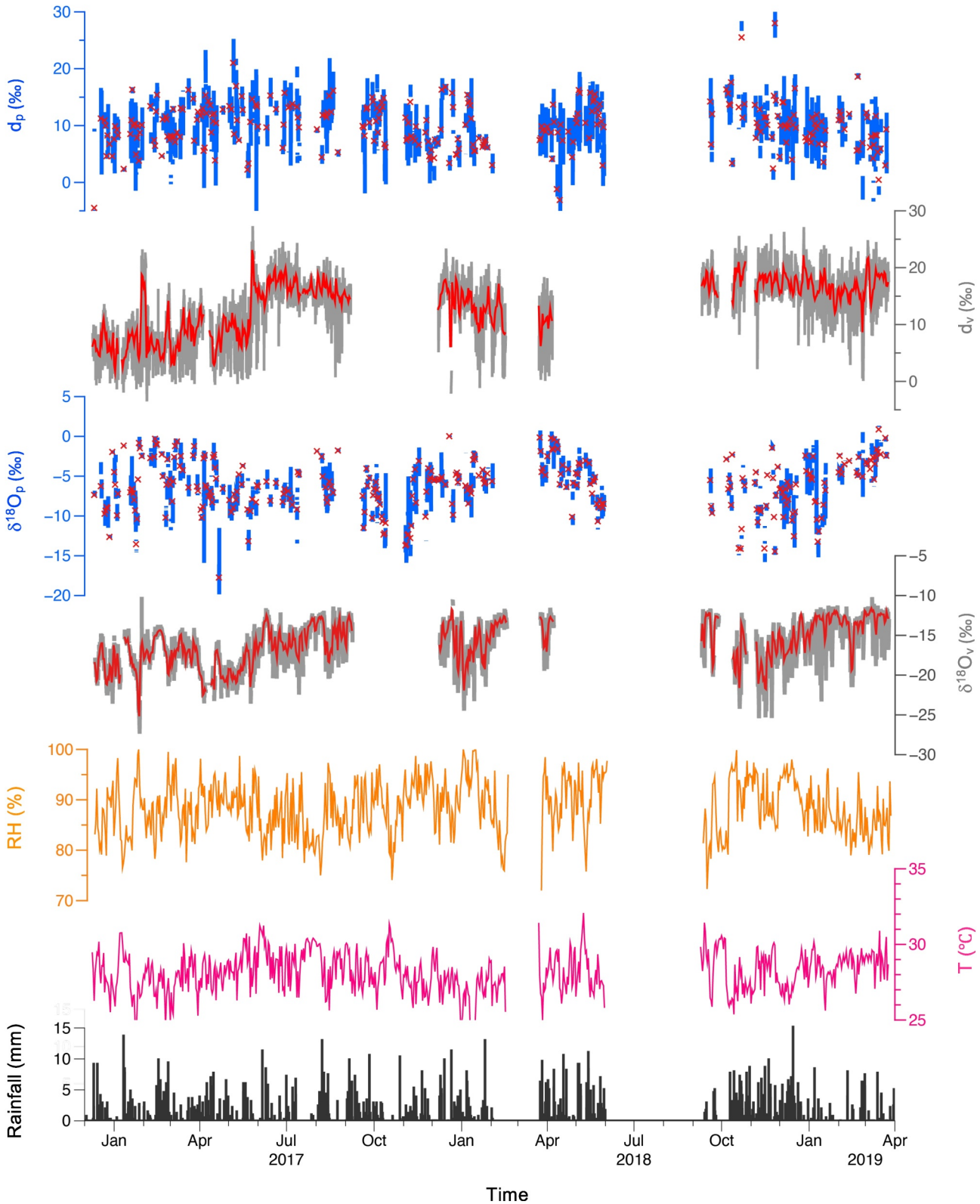

Figure 2. Time series of oxygen isotopes and d-excess of rain ($\delta^{18}O_p$ and d_p) and vapor ($\delta^{18}O_v$ and d_v) along with on-site meteorological parameters, relative humidity, temperature (T), and rainfall. Meteorological parameters are daily average, and rain and vapor isotopes include both minute data and daily average (red). The data gaps in the time series signify instrument failure.

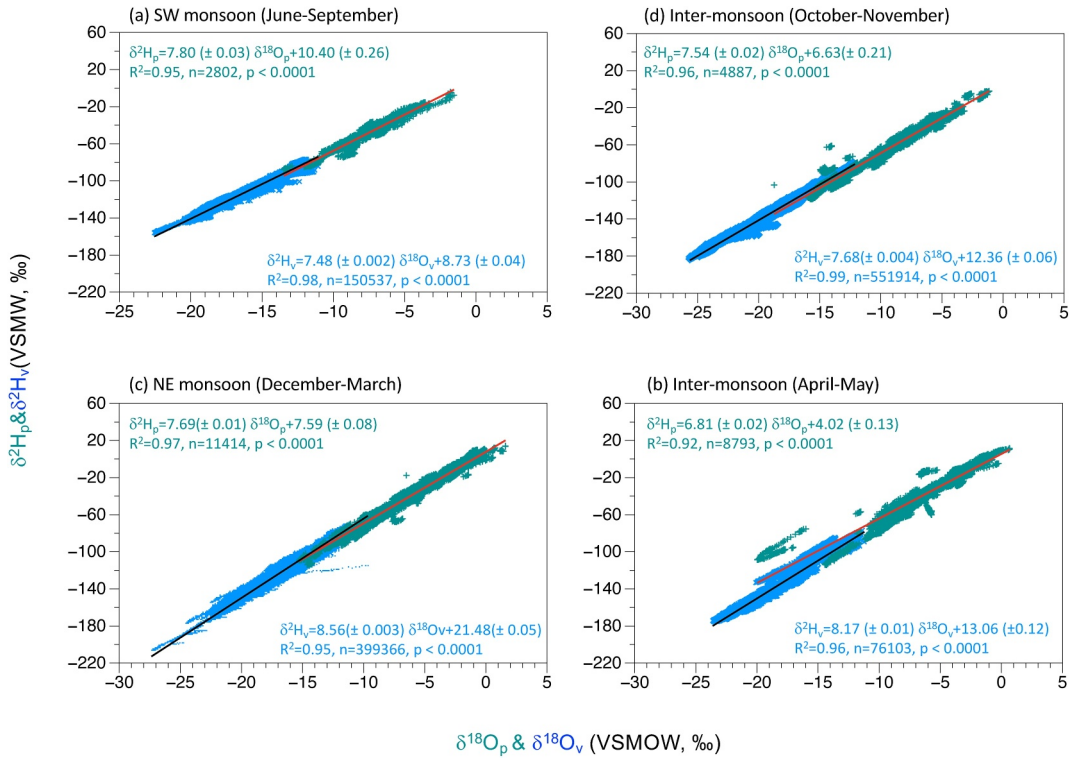

Figure 3. Local meteorological water line (LMWL; red) and local vapor line (LVL; black) during (a) SW monsoon (June–September), (b) inter-monsoon (October–November), (c) NE monsoon (December–March), and (d) inter-monsoon (April–May). *n* represents the number of data points.

$$\delta^2H_p = 7.80(\pm0.03)\,\delta^{18}O_p + 10.40(\pm0.26)\,(R^2 = 0.95) \quad (5)$$

During the NE monsoon and inter-monsoon seasons, the slopes and the intercepts of the LMWLs are smaller compared to the GMWL. In particular, during the April–May inter-monsoon, the LMWL has the smallest slope and intercept. The following are the LMWLs during the NE monsoon (Equation 6), the October–November inter-monsoon (Equation 7), and the April–May inter-monsoon (Equation 8), respectively:

$$\delta^2H_p = 7.54(\pm0.02)\,\delta^{18}O_p + 6.63(\pm0.21)\,(R^2 = 0.96) \quad (6)$$

$$\delta^2H_p = 7.69(\pm0.01)\,\delta^{18}O_p + 7.59(\pm0.08)\,(R^2 = 0.97) \quad (7)$$

$$\delta^2H_p = 6.82(\pm0.02)\,\delta^{18}O_p + 4.02(\pm0.13)\,(R^2 = 0.92) \quad (8)$$

In general, the LVLs have a higher slope with a larger intercept relative to the corresponding LMWLs except during the SW monsoon season when the slopes and intercepts of the LMWL and LVL are similar. The following are the LVL during the April–May inter-monsoon (Equation 9), the SW monsoon (Equation 10), the October–November inter-monsoon (Equation 11), and the NE monsoon (Equation 12), respectively:

$$\delta^2H_v = 8.17(\pm0.01)\,\delta^{18}O_v + 13.06(\pm0.12)\,(R^2 = 0.96) \quad (9)$$

$$\delta^2H_v = 7.48(\pm0.002)\,\delta^{18}O_v + 8.73(\pm0.04)\,(R^2 = 0.98) \quad (10)$$

$$\delta^2H_v = 7.68(\pm0.004)\,\delta^{18}O_v + 12.36(\pm0.06)\,(R^2 = 0.99) \quad (11)$$

$$\delta^2Hv = 8.56(\pm0.003)\,\delta^{18}O_v + 21.48(\pm0.05)\,(R^2 = 0.95) \quad (12)$$

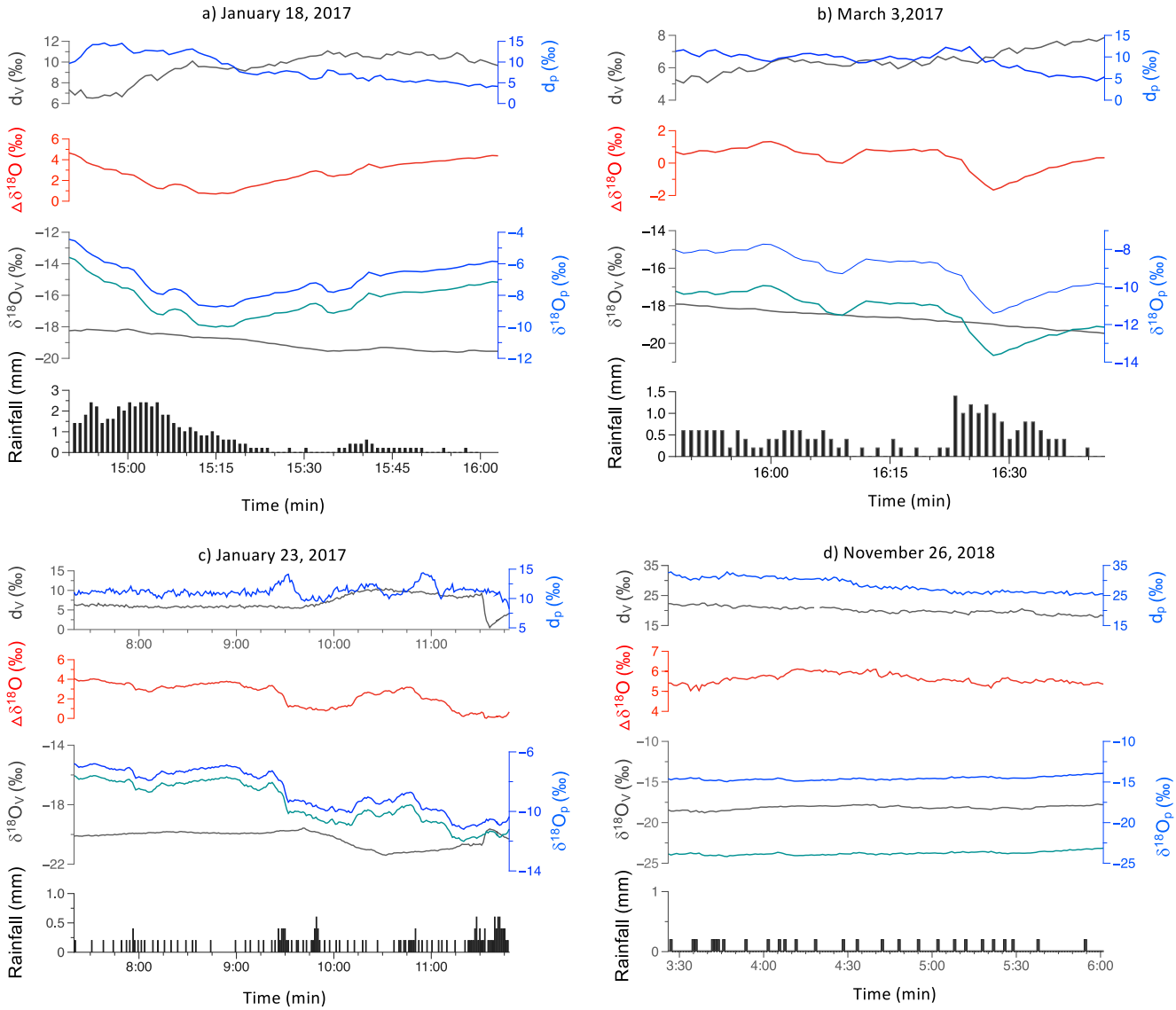

Figure 4. Evolution of $\delta^{18}O_v$, $\delta^{18}O_p$, d_v, and d_p along with rainfall amount (mm) during (a) event on 18 January 2017 (NE monsoon), (b) event on 3 March 2017 (Inter-monsoon), (c) event on 23 January 2017 (NE monsoon), and (d) event on 26 November 2018 (NE monsoon). V = vapor, p = precipitation or rain, and NE = Northeast. The green curve represents the calculated $\delta^{18}O_v$ of the vapor in equilibrium with rain.

3.3. Evolution of $\delta^{18}O$, $\delta^{2}H$, *d*-Excess, and $\Delta\delta$ During Individual Events

During a typical rain event with only one convection cell, which usually manifests as a single rainfall peak at the early stage of events (He, Goodkin, Kurita, et al., 2018), such as the event on 18 Jan 2017, $\delta^{18}O_p$ exhibits a "V" shape with the lowest values observed in the middle of the event, whereas $\delta^{18}O_v$ shows less variability (Figure 4a). The variation in $\Delta\delta^{18}O$ follows that of $\delta^{18}O_p$ with a similar "V" shape. d_v and d_p are anticorrelated ($r = -0.80$, $p < 0.0001$); in general, d_p decreases toward the end of the event in opposition to an increase in dv. The lowest isotope value of rain does not occur in the convection zone with the largest rainfall but largely in the transition zone between the convection and the stratiform zone or in the early stratiform zone (Figure 4; He, Goodkin, Jackisch, et al., 2018; He, Goodkin, Kurita, et al., 2018). The condensation height of precipitation in the stratiform zone is higher than that in the convection zone (He, Goodkin, Kurita, et al., 2018; Risi et al., 2010), and thus precipitation tends to have a lower isotope value. Downdraft also brings cold isotopically depleted vapor into the sub-cloud layer to reduce $\delta^{18}O_p$ (Kurita, 2013).

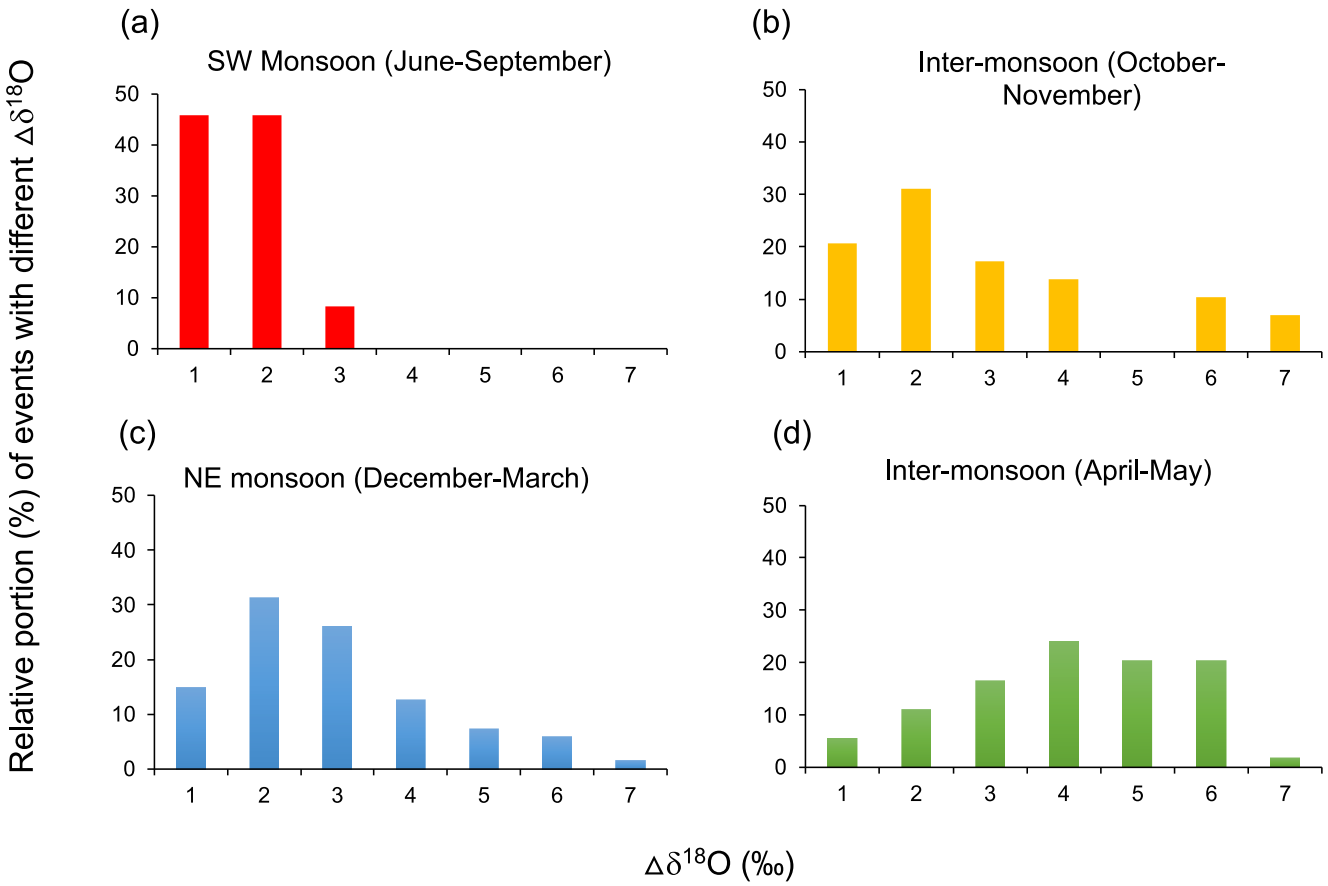

Figure 5. Distribution of events with different ranges of $\Delta\delta^{18}O$ (in absolute value) during (a) SW monsoon (June –September), (b) inter-monsoon (October–November), (c) NE monsoon (December–March), and (d) inter-monsoon (April–May). $\Delta\delta^{18}O$ = equilibrium vapor $\delta^{18}O$ − measured vapor $\delta^{18}O$.

The evolution pattern of stable isotopes during an event with multiple convection cells (with more than one rainfall peak) is more complicated, for example, the event on 3 March 2017 (Figure 4b); its $\delta^{18}O_p$ and $\Delta\delta^{18}O$ show a "W" shape. The anticorrelation between d_v and d_p is also observed during this event ($r = 0.83$, $p < 0.0001$). During stratiform rain events, the stable isotopes as well as d-excess and $\Delta\delta^{18}O$ do not change much without "V" or "W" shapes (Figure 4d). The event on 23 January 2017 was a combination of a stratiform rain at the early stage and rain associated with multiple convention cells with a "W" shape at the late stage (Figure 4c).

3.4. Distribution of Rain Events With Different Ranges of Δδ and Rainfall

Both $\Delta\delta^{18}O$ and $\Delta\delta^{2}H$ of the 324 rain events monitored in this study vary considerably (Table S2 in Supporting Information S1); $\Delta\delta^{18}O$ ranges from −2.56 to 11.18‰ with an average of 2.29‰ and $\Delta\delta^{2}H$ from −19.58 to 77.02‰ with an average of 18.67‰. On an event scale (event average), $\Delta\delta^{18}O$ ranges from 0.1% to 7.37% and $\Delta\delta^{2}H$ from 1.04 to 58.94‰. Like $\delta^{18}O$ and $\delta^{2}H$, $\Delta\delta^{18}O$ and $\Delta\delta^{2}H$ are not correlated with on-site meteorological parameters.

Only about 19% of the events have a $\Delta\delta^{18}O$ of 0–1‰ (hereafter $\Delta\delta^{18}O$ is expressed in absolute value) close to equilibrium, whereas most events (81%) have a $\Delta\delta^{18}O$ greater than 1‰. The relative portion of events with different ranges of $\Delta\delta^{18}O$ varies seasonally (Figure 5). During monsoon seasons, particularly the SW monsoon, nearly 50% of events have a $\Delta\delta^{18}O$ less than 1‰ (Figure 5a). On the other hand, during inter-monsoon seasons, there are more events with a much larger $\Delta\delta^{18}O$. For example, during the April–May inter-monsoon, more than 95% of events exhibit a $\Delta\delta^{18}O$ larger than 1‰ (Figures 5b and 5d). Additionally, relative to the SW monsoon, there are more events with higher $\Delta\delta^{18}O$ during the NE monsoon (Figure 5a).

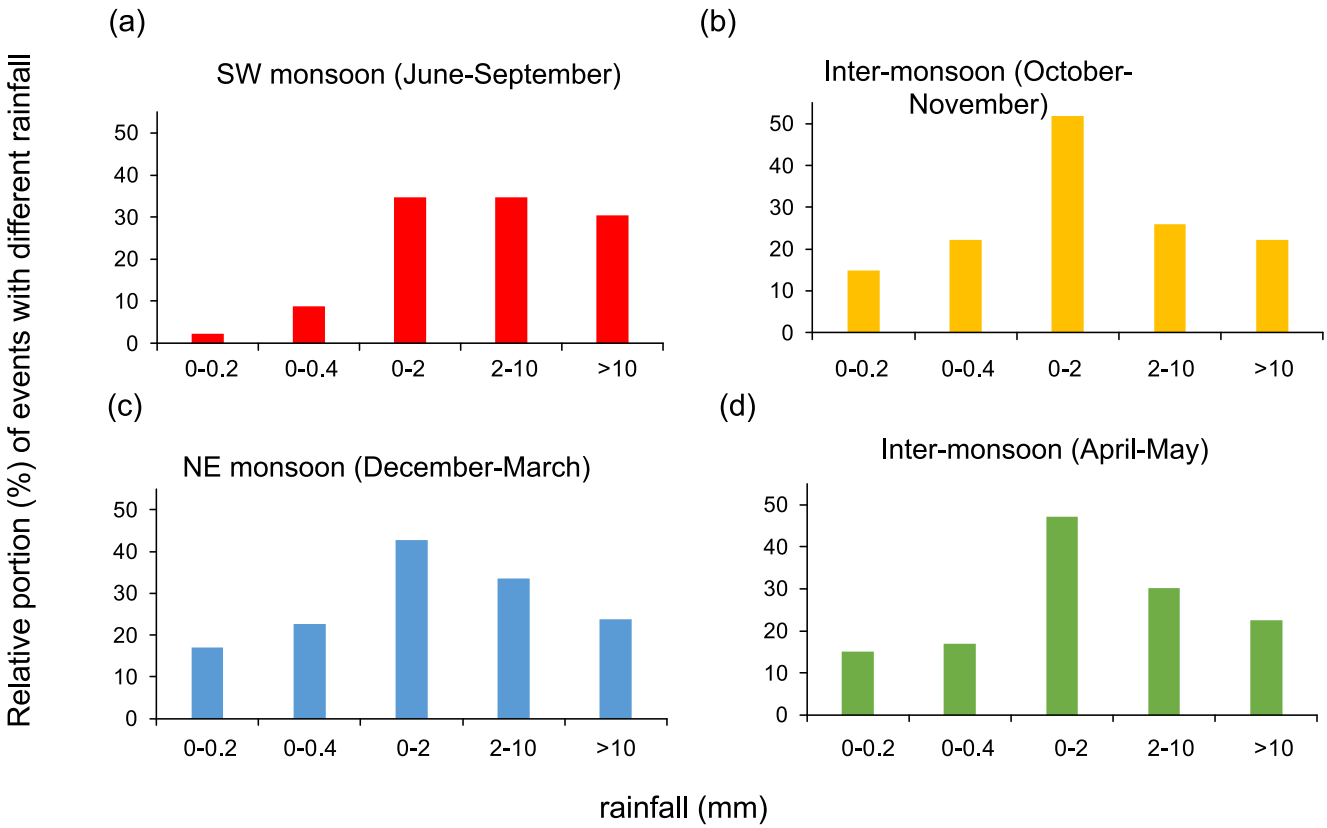

Figure 6. Distribution of events with different ranges of rainfall (a) SW monsoon (June–September), (b) inter-monsoon (October–November), (c) NE monsoon (December–March), and (d) inter-monsoon (April–May).

Similar to the patterns observed with $\Delta\delta^{18}O$, the relative portion of events with different ranges of rainfall also changes seasonally (Figure 6; Table S2 in Supporting Information S1). During inter-monsoon seasons, there is generally a high frequency of events with light rain. For example, during April–May inter-monsoon, approximately 50% of events experience light rain with rainfall below 2 mm, and more than 30% of these events exhibit extremely light rain with rainfall below 0.2 mm. In contrast, during the June–September monsoon, over 65% of rain events exceed 2 mm, whereas only 34% of events have rainfall below 2 mm, with only 5% of them being extremely light rain with rainfall below 0.2 mm.

4. Discussions

4.1. Below-Cloud Rain-Vapor Interactions as a Major Driver of Rain and Vapor Isotopes

The majority of events (81%) in our study have a $\Delta\delta^{18}O$ value larger than 1‰ (Table S2 in Supporting Information S1 and Figure 5), suggesting that, in general, rain and vapor did not reach isotopic equilibrium. In line with the previous studies (He, Goodkin, Jackisch, et al., 2018; He, Goodkin, Kurita, et al., 2018; He et al., 2021), rain and vapor isotopes, including $\Delta\delta^{18}O$, during rain events in this study exhibit low to no correlation with on-site meteorological parameters. This suggests that rain and vapor isotopes as well as $\Delta\delta^{18}O$ variability should be primarily governed by atmospheric conditions (i.e., RH) and below cloud rain-vapor interactions rather than on-site ground conditions. In a moist environment with more rainfall (Figure 7), rain-vapor diffusion exchange is prevalent, driving isotopic equilibrium between rain and vapor. Conversely, under dry conditions, raindrop evaporation becomes important, resulting in higher isotope values in rain but lower isotope values in vapor. Given the general lack of isotope equilibrium between vapor and rain, raindrop evaporation was more prevalent relative to rain-vapor diffusion exchange during the rain events examined in this study.

The change in the relative distribution of events with different ranges of $\Delta\delta^{18}O$ and rainfall during different seasons reflect the seasonal change in the relative importance of evaporation and rain-vapor diffusion exchange

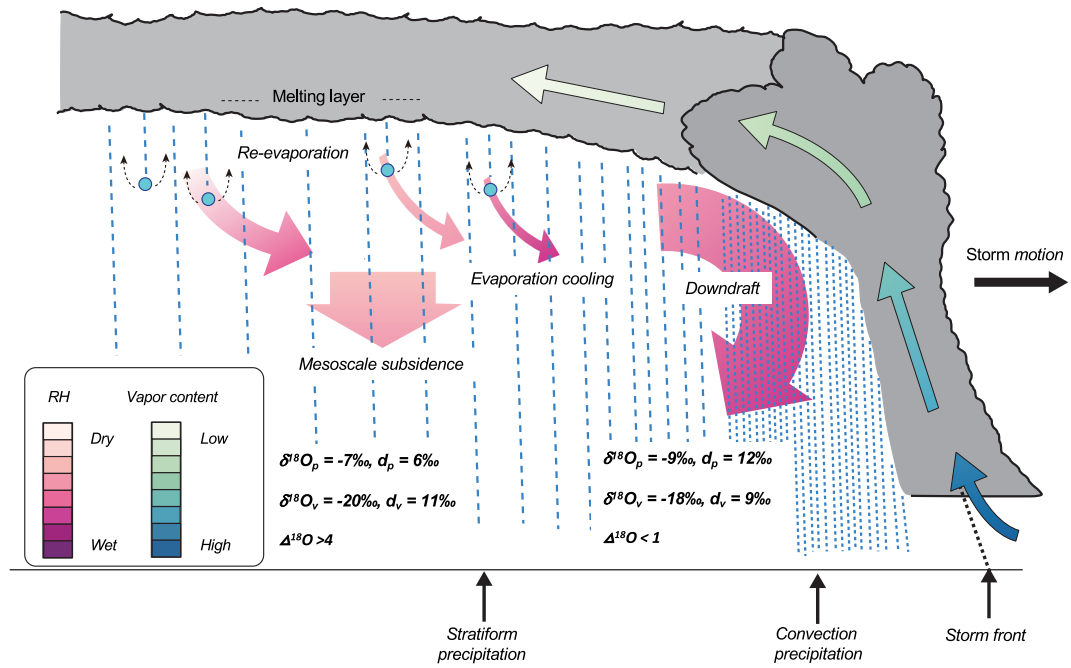

Figure 7. Schematic of a convection event with major components (modified from He, Goodkin, Kurita, et al., 2018). In the early stage, characterized by relatively large rainfall and high humidity, diffusion exchange is more influential, driving rain and vapor isotopes toward equilibrium. In the late stage, characterized by light rain and low humidity, rain evaporation becomes the dominant process, leading to a larger isotope disequilibrium.

(Figures 5 and 6). Although Singapore typically experiences a tropical climate with abundant rainfall and high humidity throughout the year, the monsoon seasons, characterized by increased regional convective activities (He, Goodkin, Jackisch, et al., 2018; He, Goodkin, Kurita, et al., 2018; He et al., 2021), feature a higher frequency of large rain events and thus relatively higher humidity below cloud base. Such a condition facilitates isotopic equilibrium between rain and vapor. During the SW monsoon, for example, nearly 70% of rain events have medium to high-intensity rainfall with amounts exceeding 2 mm (Figure 6a). Not surprisingly, over 45% of observed rain events exhibit a $\Delta\delta^{18}O$ value lower than 1‰, with only a few (8%) having a $\Delta\delta^{18}O$ value larger than 2‰ and no event's $\Delta\delta^{18}O$ larger than 3‰ (Figure 5a). As stated earlier, we consider vapor and rain during events with $\Delta\delta^{18}O$ values lower than 1‰ to be close to isotopic equilibrium.

In contrast, during inter-monsoons, rain events, with a significant portion having extremely low rainfall below 0.2 mm (Figures 6b and 6d), are largely associated with local convection. Compared to those in monsoon seasons, the below-cloud environments of inter-monsoon events tend to have relatively lower humidity, leading to the dominance of evaporation. For example, during April–May inter-monsoon, the majority of rain events (95%) have a $\Delta\delta^{18}O$ larger than 1‰, with only a small number of rain events (5%) having a $\Delta\delta^{18}O$ value below 1‰ (Figure 4d). Similarly to the SW monsoon, the NE monsoon has a significant portion of events with higher rainfall (Figure 6c). However, there are also a large number of local events with rainfall less than 2 mm or even 0.2 mm. These small events largely occurred in the last or dry phase of the NE monsoon, that is, February and March. Therefore, the NE monsoons have more events with a larger $\Delta\delta^{18}O$.

Like $\Delta\delta^{18}O$, the slopes of the LMWLs and LVLs and their seasonal changes also record the impact of below-cloud processes on rain and vapor isotopes (Figure 3). Relatively high humidity conditions below cloud base in the majority of rain events during monsoon seasons, in particular, the SW monsoon, favors rain-vapor isotope equilibrium. Therefore, the LMWL and LVL during this period have slopes close to that of the GLMWL, and also the difference between them is small (Figure 3a). In contrast, under relatively low humidity conditions below cloud base of most rain events during inter-monsoon periods, raindrop evaporation dominates over rain-vapor equilibrium, resulting in higher isotope values and lower d-excess in rainwater and thus a lower slope of the LMWL. The impact of evaporation on the stable isotopes of rain and vapor is the opposite; it increases (decreases) isotope values in rain (vapor) but decreases (increases) d-excess in rain (vapor). For example, during the events on

Jan 18 and 3 March 2017 (Figure 4a), rain evaporation gradually increased $\delta^{18}O_p$ but decreased $\delta^{18}O_v$ with their d-excess values exhibiting negative correlations ($r = -0.79$ and $r = -0.83$, respectively) (Figures 4a and 4b). In our region, the LVL tends to have a steeper slope but a larger intercept than the concurrent LMWL. Stronger evaporation also results in a larger difference between the slopes of the LVL and LMWL, which, for example, can be observed during the April–May inter-monsoon (Figure 3b). During the late dry stage of the NE monsoon, the area experiences a dry condition with less rain or more extremely light rains but receives more rain during October–November inter-monsoon, especially in November, compared to the April–May inter-monsoon. The difference between the slopes of the LMWL and LVL during these two periods falls between the differences observed during the SW monsoon and the April–May inter-monsoon.

4.2. Effect of Rain-Vapor Interaction on the Evolution of Their Isotopes During Individual Events

Below cloud rain-vapor interactions also play an important role in the evolution of the stable isotopes of both rain and vapor during individual rain events. As depicted in Figure 7, below-cloud RH conditions, along with other parameters such as rainfall rate and raindrop sizes, will not remain the same but vary during a typical tropical rain event. These fluctuations affect rain-vapor interaction and alter the relative importance of rain evaporation and diffusion exchange. At the very early stage of convection, with relatively large raindrops and a high rainfall rate, the influence of rain-vapor interaction on their isotopes is minimal. At the late stage of convection, as the event progresses into the stratiform zone, where the rain rate decreases, especially toward the end of an event, and humidity drops, raindrop evaporation gains prominence. As a result, $\delta^{18}O_p$ increases and d_p decreases but d_v increases (Figures 5a and 5b), leading to a negative correlation between d_p and d_v. $\Delta\delta^{18}O$ is generally small during the middle of a rain event when humidity still remains at a relatively high level, but it becomes larger with a decrease in humidity at the late stage of events.

Graf et al. (2019) employed a simple column model to simulate the evolution of stable isotopes of rain and vapor, specifically, $\Delta\delta^2H$ and Δd during a rain event during precipitation. This model considers several factors that might affect rain-vapor interaction, including temperature, RH, and raindrop size as well as initial isotope values, and demonstrate how these affect rain and vapor interaction and their isotopes, that is, $\Delta\delta^2H$ and Δd. They proposed a framework, a $\Delta\delta - \Delta d$ diagram, to evaluate the deviation of vapor and rain from isotopic equilibrium. A negative $\Delta\delta^2H$ indicates that rain is more depleted in ^2H than ambient water vapor, and the rain isotopes still largely reflect the conditions inside clouds. However, raindrop evaporation below the cloud base introduces kinetic fractionation, leading to more positive $\Delta\delta^2H$ especially for small raindrops (Lee & Fung, 2008). Therefore, equilibrium and evaporation lead to different pathways in this $\Delta\delta - \Delta d$ diagram, which provides a qualitative way to identify below-cloud processes (Graf et al., 2019). Their sensitivity testing by altering initial parameters, including raindrop sizes, RH, T, isotope values, and condensation height, largely resembles the varying conditions during the 324 events monitored in this study. Figure 6, a $\Delta\delta - \Delta d$ diagram including $\Delta\delta^2H_v$ and Δd_v of randomly selected rain events from this study, clearly illustrates the influence of evaporation on rain and vapor isotopes during these events.

The evolution of $\Delta\delta^2H$ and Δd during the event on 22 May 2017 (blue-purple solid diamonds in Figure 8; Figure S5 in Supporting Information S1) exemplifies how these below-cloud processes impact the stable isotopes of rain and vapor. Initially, at the early stage of this event, the influence of below-cloud processes on raindrops was relatively minimal likely due to a higher portion of large-sized raindrops and a high rain rate (Bolin, 1958; Lee & Fung, 2008). As a result, raindrops still retained much of the cloud signals, leading to samples primarily situated in the left quadrants in Figure 8. As the event progressed, with humidity still relatively high during the middle event, rain-vapor diffusion exchange prevailed, establishing a close equilibrium between rain and vapor isotopes with both $\Delta\delta^2H_v$ and Δd_v being generally close to zero. Subsequently, during the late stage, with diminished rainfall, reduced rain rate, and smaller droplets, evaporation gained significance, leading to a deviation of rain and vapor isotopes from equilibrium and a predominant distribution of the samples in the right quadrants. Near the end of the event, another convection cell passed by the site bringing heavy rainfall (the second rainfall peak between 7:00 p.m. and 8:00 p.m. in Figure S5 in Supporting Information S1), facilitating rain-vapor diffusion exchange and shifting both $\Delta\delta^2H_v$ and Δd_v to zero. After this short rainfall peak, a slowdown in rainfall and a decrease in raindrop sizes led to rain evaporation becoming dominant again. Therefore, the samples are largely located in the lower right quadrant in Figure 8. This example vividly demonstrates how the interplay of rain rate, droplet size, and humidity conditions modulates the rain-vapor interaction, thus influencing their isotopes.

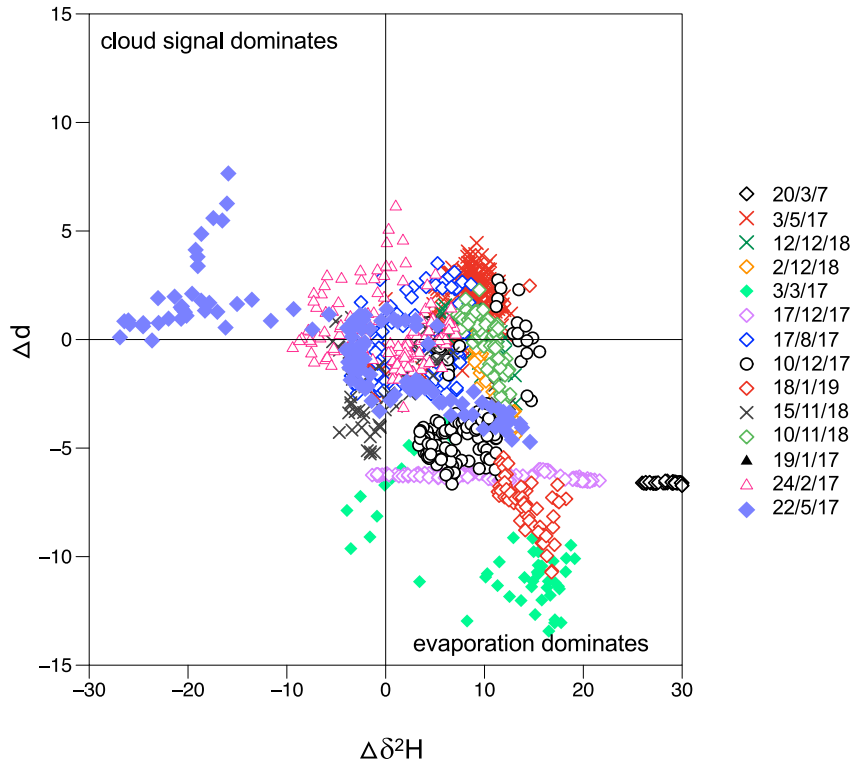

Figure 8. ΔδΔd-diagram (based on Graf et al., 2019) of randomly selected rain events investigated in this study. Samples plotted in the left quadrants largely keep cloud signal and those in the right quadrants are significantly affected by evaporation.

4.3. Controls of Regional Convection on the Long-Term Evolution of Rain and Vapor Isotopes

To investigate the influence of convective activity, we analyzed the correlation of vapor and rain isotopes with the OLR over the region. OLR has been used as a proxy for deep tropical convection, where low OLR values suggest enhanced convection (Vimeux et al., 2011). Our analysis reveals a strong positive correlation between vapor and rain isotopes and regional OLR, and therefore low $\delta^{18}O$ corresponds to strong convection with low OLR (Figure 9). Notably, the correlation is much stronger for monthly $\delta^{18}O$ (Figures 7c and 7d) than that for daily average $\delta^{18}O$ (Figures 9a and 9b). This arises because daily sample's isotopes are more affected by local factors and convective processes, whereas on monthly scales, large climate systems such as monsoons exert more influence (He, Goodkin, Kurita, et al., 2018). On longer timescales, the regional convection controls the variability of vapor and rain $\delta^{18}O$, such as seasonal variability (Figure 3 and Figure S2 in Supporting Information S1). During the two monsoon seasons (i.e., the SW and NE monsoons) that the study region experiences, the intertropical convergence zone passes the region, bringing more rainfall with stronger regional convection. Stronger regional convection also leads to seasonal negative shifts observed in the time series of rain and vapor isotopes around two monsoon periods (Figure 2 and Figure S2 in Supporting Information S1). We also observed that the correlation is generally higher for rain isotopes than for vapor isotopes. This difference in correlation can be attributed to the varying influence of environmental conditions and processes on rain and vapor despite their shared origin in the water cycle. For example, rain isotopes may be more strongly influenced by condensation or cloud dynamics. Additionally, vapor data encompass days without rainfall, which likely contributes to the observed differences in the correlation of OLR with rain and vapor isotopes.

In contrast to the positive correlation of rain and vapor $\delta^{18}O$ with the OLR over the study region, $\delta^{18}O$ shows a negative correlation with the OLR in the tropical Pacific region (Figure S6 in Supporting Information S1). Notably, the negative correlation is stronger for the monthly average $\delta^{18}O$ (Figures S3c and S3d in Supporting Information S1) compared to the daily average $\delta^{18}O$ (Figures S6a and S6b in Supporting Information S1). The change in sea surface temperature (SST) in the tropical Pacific drives convection in tropical regions (He et al., 2021; Li & Ting, 2015). The El Niño Southern Oscillation (ENSO) alters SST across the tropical Pacific and

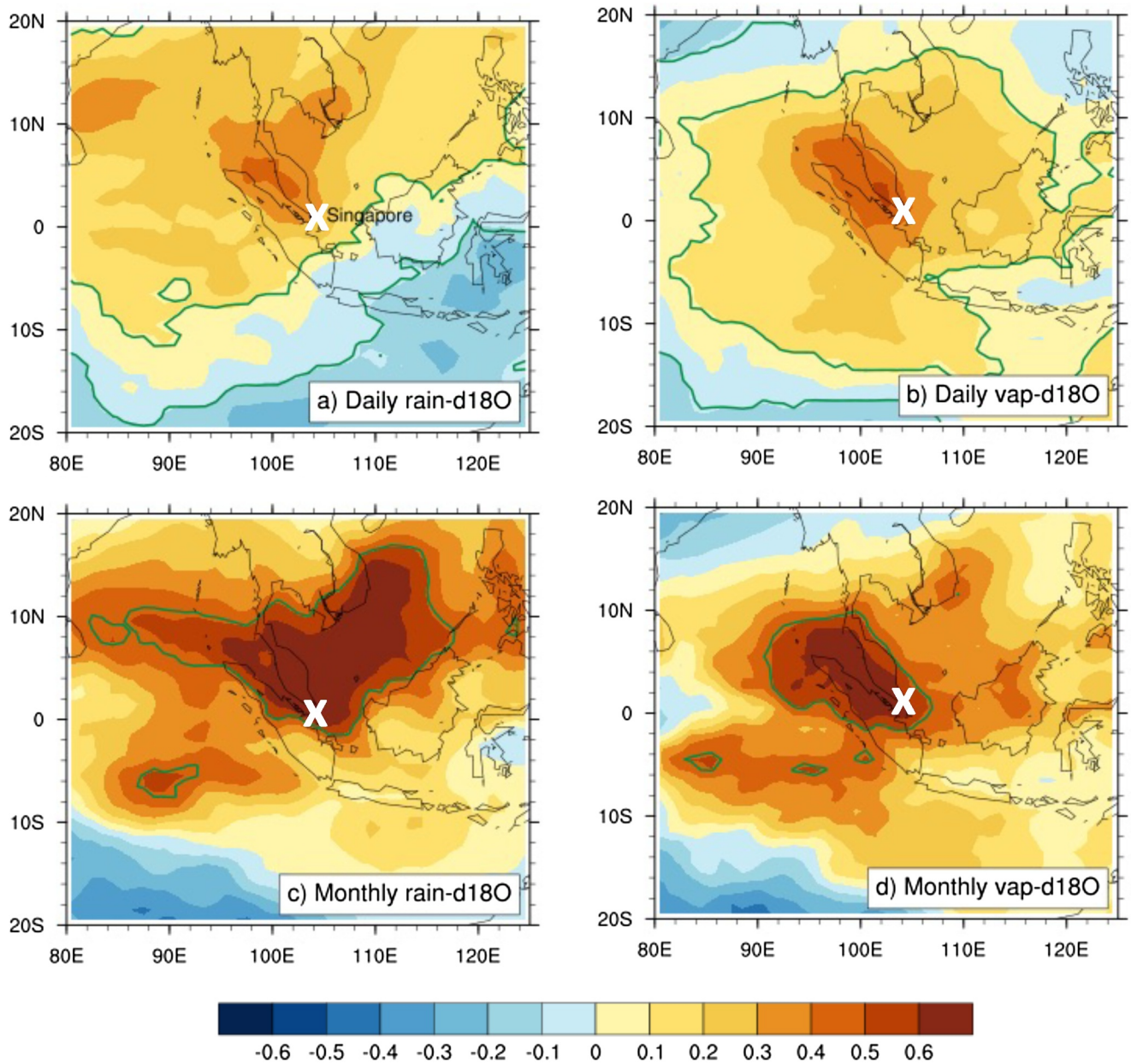

Figure 9. Correlation map of daily average $\delta^{18}O$ of rain (a) and vapor (b) and monthly average $\delta^{18}O$ of rain (c) and vapor (d) with Outgoing longwave radiation in the Southeast Asian region.

affects global weather via atmospheric teleconnections (e.g., Ashok & Yamagata, 2009). Specifically, during La Niña years, the atmospheric convection is relatively stronger over Southeast (SE) Asia. Conversely, during El Niño years, the situation is opposite with weaker convection over Southeast Asia. ENSO could, therefore, potentially influence the intraannual variation in $\delta^{18}O$ of both rain and vapor (Figure 2). However, the period covered by this study is too short for us to delve deeper into the relationship between ENSO and $\delta^{18}O$.

5. Conclusions

In this study, we present a novel approach to measure real-time rain and vapor isotopes at minute intervals continuously and simultaneously, without the need for discrete sample collection, during rain events in Singapore from Dec-2016 to Mar-2019. The majority of events (81%) with a $\Delta\delta^{18}O$ larger than 1‰ suggest that, below cloud base, isotopic equilibrium between rain and vapor was mostly not reached, indicating that raindrop

evaporation generally played a more important role than rain-vapor diffusive exchange. Seasonal variations in the relative distribution of events with different ranges of $\Delta\delta^{18}O$ and rainfall amount reflect the changing importance of rain-vapor diffusive exchange and raindrop evaporation. During monsoon seasons, a higher frequency of large rain events with greater rainfall likely helps to maintain generally high humidity below cloud base during these rain events. This condition facilitates rain-vapor diffusion exchange, leading to a closer isotopic equilibrium between rain and vapor with a greater portion of events having a small $\Delta\delta^{18}O$. In contrast, small rain events with very light rainfall or even extremely light rainfall often occur during inter-monsoon periods. Consequently, generally low humidity prevailed below cloud base during these rain events. Low humidity condition favors rain evaporation, resulting in a predominance of events with a large $\Delta\delta^{18}O$. The slopes of the LMWL and LVL also reflect below cloud rain-vapor interaction. As rain and vapor isotopes are in close equilibrium during monsoon seasons, the slopes of the LMWL and LVL align closely with that of the GMWL, but due to evaporation during inter-monsoon periods, the slopes of the LMWL are smaller than that of GMWL. A detailed examination of individual rain events reveals the important role played by below cloud rain-vapor interaction in shaping the evolution of rain and vapor isotopes. At the early stage of an event, high rain rates and large droplet sizes limit the influence of below-cloud processes, allowing rainwater to retain cloud information with $\Delta\delta^{2}H$ and $\Delta\delta^{18}O$ being negative. As rain events progress and rainfall slows down, raindrop evaporation becomes important under low humidity conditions, leading to positive $\Delta\delta^{2}H$ and $\Delta\delta^{18}O$. In conclusion, our study provides compelling evidence that below-cloud processes, specifically rain-vapor interactions, are a major driver of rain and vapor isotopes, and that high-resolution minute isotope data of rain and vapor can provide valuable constraints on these below-cloud processes, which are otherwise challenging to measure accurately.

Both rain and vapor isotopes exhibit a strong correlation with regional convection. During the NE and SW monsoons, intensified convection leads to lower rain and vapor isotopes, causing negative shifts in their time series. Additionally, the negative correlation of $\delta^{18}O_p$ and $\delta^{18}O_v$ with the OLR in the tropical Pacific region suggests a possible influence of ENSO. It is worth noting, however, that the duration of our study period is not long enough to provide a comprehensive understanding of the impact of interannual climate variability such as ENSO on the stable isotope of rain and vapor. A longer data record is needed to explore this relationship in greater detail.

Data Availability Statement

The stable isotope values of vapor and rain monitored during this investigation between 2016 and 2019 can be accessed at He et al. (2024). Additionally, on-site meteorological parameters, including temperature, relative humidity, and rainfall amount, are included in the same data set. The data collected in this investigation are also available by contacting the authors. Reanalysis data used in this study are freely available from their respective sources as detailed in Section 2.3.

Acknowledgments
We would like to express our gratitude to Bernie Wee Wei Ken for making Figure 1 and to Wei Jia and Yunyue Yang for making Figure S2 in Supporting Information S1. Special thanks are extended to Clarice Teo Jia Wen for her assistance in processing the raw data of rain and vapor from Picarro water analyzers. We are also grateful to three anonymous reviewers for providing constructive feedback that significantly helped to improve the quality of our manuscript. The authors gratefully acknowledge the financial support provided by the Singapore Ministry of Education (Grant MOE-MOET2EP10121-0008). This research is also supported by the National Research Foundation Singapore and the Singapore Ministry of Education under the Research Centers of Excellence initiative. It comprises Earth Observatory of Singapore contribution no. 528.

References

Aemisegger, F., Spiegel, J. K., Pfahl, S., Sodemann, H., Eugster, W., & Wernli, H. (2015). Isotope meteorology of cold front passages: A case study combining observations and modeling: Water isotopes during cold fronts. *Geophysical Research Letters*, *42*(13), 5652–5660. https://doi.org/10.1002/2015GL063988

Angert, A., Lee, J.-E., & Yakir, D. (2008). Seasonal variations in the isotopic composition of near-surface water vapour in the eastern Mediterranean. *Tellus B: Chemical and Physical Meteorology*, *60*(4), 674–684. https://doi.org/10.1111/j.1600-0889.2008.00357.x

Ashok, K., & Yamagata, T. (2009). Climate change: The El Nino with a difference. *Nature*, *461*(7263), 481–484. https://doi.org/10.1038/461481a

Benetti, M., Lacour, J.-L., Sveinbjörnsdóttir, A. E., Aloisi, G., Reverdin, G., Risi, C., et al. (2018). A framework to study mixing processes in the marine boundary layer using water vapor isotope measurements. *Geophysical Research Letters*, *45*(5), 2524–2532. https://doi.org/10.1002/2018GL077167

Bhattacharya, S. K., Sarkar, A., & Liang, M.-C. (2022). Vapor isotope probing of typhoons invading the Taiwan region in 2016. *Journal of Geophysical Research: Atmospheres*, *127*(21), e2022JD036578. https://doi.org/10.1029/2022JD036578

Bolin, B. (1958). On the use of tritium as a tracer for water in nature. *Proceedings of 2nd International Conference on Peaceful Use of Atomic Energy*, *18*, 336–343.

Bonne, J.-L., Behrens, M., Meyer, H., Kipfstuhl, S., Rabe, B., Schönicke, L., et al. (2019). Resolving the controls of water vapour isotopes in the Atlantic sector. *Nature Communications*, *10*(1), 1632. https://doi.org/10.1038/s41467-019-09242-6

Casado, M., Landais, A., Masson-Delmotte, V., Genthon, C., Kerstel, E., Kassi, S., et al. (2016). Continuous measurements of isotopic composition of water vapour on the East Antarctic Plateau. *Atmospheric Chemistry and Physics*, *16*(13), 8521–8538. https://doi.org/10.5194/acp-16-8521-2016

Conroy, J. L., Noone, D., Cobb, K. M., Moerman, J. W., & Konecky, B. L. (2016). Paired stable isotopologues in precipitation and vapor: A case study of the amount effect within western tropical Pacific storms. *Journal of Geophysical Research: Atmospheres*, *121*(7), 3290–3303. https://doi.org/10.1002/2015JD023844

Craig, H. (1961). Isotopic variations in meteoric waters. *Science*, *133*(3465), 1702–1703. https://doi.org/10.1126/science.133.3465.1702

Dai, D., Gao, J., Steen-Larsen, H. C., Yao, T., Ma, Y., Zhu, M., & Li, S. (2021). Continuous monitoring of the isotopic composition of surface water vapor at Lhasa, southern Tibetan Plateau. *Atmospheric Research*, *264*, 105827. https://doi.org/10.1016/j.atmosres.2021.105827

Dansgaard, W. (1964). Stable isotopes in precipitation. *Tellus*, *16*(4), 436–468. https://doi.org/10.1111/j.2153-3490.1964.tb00181.x

Dee, S., Bailey, A., Conroy, J. L., Atwood, A., Stevenson, S., Nusbaumer, J., & Noone, D. (2023). Water isotopes, climate variability, and the hydrological cycle: Recent advances and new frontiers. *Environmental Research: Climate*, *2*(2), 022002. https://doi.org/10.1088/2752-5295/accbe1

Deshpande, R. D., Maurya, A. S., Kumar, B., Sarkar, A., & Gupta, S. K. (2010). Rain-vapor interaction and vapor source identification using stable isotopes from semiarid western India. *Journal of Geophysical Research*, *115*(D23), 2010JD014458. https://doi.org/10.1029/2010JD014458

Field, R. D., Kim, D., LeGrande, A. N., Worden, J., Kelley, M., & Schmidt, G. A. (2014). Evaluating climate model performance in the tropics with retrievals of water isotopic composition from Aura TES. *Geophysical Research Letters*, *41*(16), 6030–6036. https://doi.org/10.1002/2014GL060572

Fiorella, R. P., Poulsen, C. J., & Matheny, A. M. (2018). Seasonal patterns of water cycling in a deep, continental mountain valley inferred from stable water vapor isotopes. *Journal of Geophysical Research: Atmospheres*, *123*(14), 7271–7291. https://doi.org/10.1029/2017JD028093

Fiorella, R. P., West, J. B., & Bowen, G. J. (2019). Biased estimates of the isotope ratios of steady-state evaporation from the assumption of equilibrium between vapour and precipitation. *Hydrological Processes*, *33*(19), 2576–2590. https://doi.org/10.1002/hyp.13531

Galewsky, J., Rella, C., Sharp, Z., Samuels, K., & Ward, D. (2011). Surface measurements of upper tropospheric water vapor isotopic composition on the Chajnantor Plateau, Chile: Chile water vapor isotopic composition. *Geophysical Research Letters*, *38*(17). https://doi.org/10.1029/2011GL048557

Galewsky, J., Steen-Larsen, H. C., Field, R. D., Worden, J., Risi, C., & Schneider, M. (2016). Stable isotopes in atmospheric water vapor and applications to the hydrologic cycle: Isotopes in the atmospheric water cycle. *Reviews of Geophysics*, *54*(4), 809–865. https://doi.org/10.1002/2015RG000512

Gat, J. R. (1996). Oxygen and hydrogen isotopes in the hydrologic cycle. *Annual Review of Earth and Planetary Sciences*, *24*(1), 225–262. https://doi.org/10.1146/annurev.earth.24.1.225

Gibson, J. J., Birks, S. J., & Edwards, T. W. D. (2008). Global prediction of δ_A and δ^2H-$\delta^{18}O$ evaporation slopes for lakes and soil water accounting for seasonality. *Global Biogeochemical Cycles*, *22*(2). https://doi.org/10.1029/2007GB002997

González, Y., Schneider, M., Dyroff, C., Rodríguez, S., Christner, E., García, O. E., et al. (2016). Detecting moisture transport pathways to the subtropical North Atlantic free troposphere using paired H_2O-δD in situ measurements. *Atmospheric Chemistry and Physics*, *16*(7), 4251–4269. https://doi.org/10.5194/acp-16-4251-2016

Good, S. P., Noone, D., & Bowen, G. (2015). Hydrologic connectivity constrains partitioning of global terrestrial water fluxes. *Science*, *349*(6244), 175–177. https://doi.org/10.1126/science.aaa5931

Graf, P., Wernli, H., Pfahl, S., & Sodemann, H. (2019). A new interpretative framework for below-cloud effects on stable water isotopes in vapour and rain. *Atmospheric Chemistry and Physics*, *19*(2), 747–765. https://doi.org/10.5194/acp-19-747-2019

Harder, P., & Pomeroy, J. (2013). Estimating precipitation phase using a psychrometric energy balance method: Precipitation phase using a psychrometric energy balance. *Hydrological Processes*, *27*(13), 1901–1914. https://doi.org/10.1002/hyp.9799

He, S., Goodkin, N. F., Jackisch, D., Ong, M. R., & Samanta, D. (2018). Continuous real-time analysis of the isotopic composition of precipitation during tropical rain events: Insights into tropical convection. *Hydrological Processes*, *32*(11), 1531–1545. https://doi.org/10.1002/hyp.11520

He, S., Goodkin, N. F., Kurita, N., Wang, X., & Rubin, C. M. (2018). Stable isotopes of precipitation during tropical Sumatra Squalls in Singapore. *Journal of Geophysical Research: Atmospheres*, *123*(7), 3812–3829. https://doi.org/10.1002/2017JD027829

He, S., Jackisch, D., Feng, F., Samanta, D., Wang, X., & Goodkin, N. F. (2024). Rain and vapor stable isotope data collected during 324 rain events in Singapore between December 2016 and March 2019 [Dataset]. *figshare*. https://doi.org/10.6084/m9.figshare.24078489.v1

He, S., Jackisch, D., Samanta, D., Yu Yi, P. K., Liu, G., Wang, X., & Goodkin, N. F. (2021). Understanding tropical convection through triple oxygen isotopes of precipitation from the Maritime Continent. *Journal of Geophysical Research: Atmospheres*, *126*(4). https://doi.org/10.1029/2020JD033418

Horita, J., Rozanski, K., & Cohen, S. (2008). Isotope effects in the evaporation of water: A status report of the Craig–Gordon model. *Isotopes in Environmental and Health Studies*, *44*(1), 23–49. https://doi.org/10.1080/10256010801887174

Jasechko, S., Sharp, Z. D., Gibson, J. J., Birks, S. J., Yi, Y., & Fawcett, P. J. (2013). Terrestrial water fluxes dominated by transpiration. *Nature*, *496*(7445), 347–350. https://doi.org/10.1038/nature11983

Jouzel, J. (2003). Water stable isotopes: Atmospheric composition and applications in polar Ice Core Studies A2—Holland, Heinrich D. In K. K. Turekian (Ed.), *Treatise on geochemistry* (pp. 213–243). Pergamon. https://doi.org/10.1016/B0-08-043751-6/04040-8

Klein, E. S., Nolan, M., McConnell, J., Sigl, M., Cherry, J., Young, J., & Welker, J. M. (2016). McCall Glacier record of Arctic climate change: Interpreting a northern Alaska ice core with regional water isotopes. *Quaternary Science Reviews*, *131*, 274–284. https://doi.org/10.1016/j.quascirev.2015.07.030

Kurita, N. (2013). Water isotopic variability in response to mesoscale convective system over the tropical ocean. *Journal of Geophysical Research: Atmospheres*, *118*(18), 10376–10390. https://doi.org/10.1002/jgrd.50754

Lee, J., Pierrehumbert, R., Swann, A., & Lintner, B. R. (2009). Sensitivity of stable water isotopic values to convective parameterization schemes. *Geophysical Research Letters*, *36*(23), 2009GL040880. https://doi.org/10.1029/2009GL040880

Lee, J.-E., & Fung, I. (2008). "Amount effect" of water isotopes and quantitative analysis of post-condensation processes. *Hydrological Processes*, *22*(1), 1–8. https://doi.org/10.1002/hyp.6637

Lekshmy, P. R., Midhun, M., & Ramesh, R. (2018). Influence of stratiform clouds on δD and $\delta^{18}O$ of monsoon water vapour and rain at two tropical coastal stations. *Journal of Hydrology*, *563*, 354–362. https://doi.org/10.1016/j.jhydrol.2018.06.001

Lekshmy, P. R., Midhun, M., Ramesh, R., & Jani, R. A. (2014). ^{18}O depletion in monsoon rain relates to large scale organized convection rather than the amount of rainfall. *Scientific Reports*, *4*(1), 5661. PMC. https://doi.org/10.1038/srep05661

Li, X., & Ting, M. (2015). Recent and future changes in the Asian monsoon-ENSO relationship: Natural or forced? *Geophysical Research Letters*, *42*(9), 3502–3512. https://doi.org/10.1002/2015GL063557

Liu, G., Li, X., Chiang, H.-W., Cheng, H., Yuan, S., Chawchai, S., et al. (2020). On the glacial-interglacial variability of the Asian monsoon in speleothem $\delta^{18}O$ records. *Science Advances*, *6*(7), eaay8189. https://doi.org/10.1126/sciadv.aay8189

Mercer, J. J., Liefert, D. T., & Williams, D. G. (2020). Atmospheric vapour and precipitation are not in isotopic equilibrium in a continental mountain environment. *Hydrological Processes*, *34*(14), 3078–3101. https://doi.org/10.1002/hyp.13775

Moerman, J. W., Cobb, K. M., Adkins, J. F., Sodemann, H., Clark, B., & Tuen, A. A. (2013). Diurnal to interannual rainfall $\delta^{18}O$ variations in northern Borneo driven by regional hydrology. *Earth and Planetary Science Letters*, *369–370*(Supplement C), 108–119. https://doi.org/10.1016/j.epsl.2013.03.014

Muller, C. L., Baker, A., Fairchild, I. J., Kidd, C., & Boomer, I. (2014). Intra-event trends in stable isotopes: Exploring midlatitude precipitation using a vertically pointing micro rain radar. *Journal of Hydrometeorology*, *16*(1), 194–213. https://doi.org/10.1175/JHM-D-14-0038.1

Munksgaard, N. C., Kurita, N., Sánchez-Murillo, R., Ahmed, N., Araguas, L., Balachew, D. L., et al. (2019). Data Descriptor: Daily observations of stable isotope ratios of rainfall in the tropics. *Scientific Reports*, *9*(1), 14419. https://doi.org/10.1038/s41598-019-50973-9

Munksgaard, N. C., Wurster, C. M., & Bird, M. I. (2011). Continuous analysis of $\delta^{18}O$ and δD values of water by diffusion sampling cavity ring-down spectrometry: A novel sampling device for unattended field monitoring of precipitation, ground and surface waters. *Rapid Communications in Mass Spectrometry*, *25*(24), 3706–3712. https://doi.org/10.1002/rcm.5282

Nlend, B., Celle-Jeanton, H., Risi, C., Pohl, B., Huneau, F., Ngo Boum-Nkot, S., et al. (2020). Identification of processes that control the stable isotope composition of rainwater in the humid tropical West-Central Africa. *Journal of Hydrology*, *584*, 124650. https://doi.org/10.1016/j.jhydrol.2020.124650

Noone, D. (2012). Pairing measurements of the water vapor isotope ratio with humidity to deduce atmospheric moistening and dehydration in the tropical midtroposphere. *Journal of Climate*, *25*(13), 4476–4494. https://doi.org/10.1175/JCLI-D-11-00582.1

Noone, D., Risi, C., Bailey, A., Berkelhammer, M., Brown, D. P., Buenning, N., et al. (2013). Determining water sources in the boundary layer from tall tower profiles of water vapor and surface water isotope ratios after a snowstorm in Colorado. *Atmospheric Chemistry and Physics*, *13*(3), 1607–1623. https://doi.org/10.5194/acp-13-1607-2013

Nusbaumer, J., Wong, T. E., Bardeen, C., & Noone, D. (2017). Evaluating hydrological processes in the Community Atmosphere Model Version 5 (CAM5) using stable isotope ratios of water. *Journal of Advances in Modeling Earth Systems*, *9*(2), 949–977. https://doi.org/10.1002/2016MS000839

Rahul, P., Ghosh, P., Bhattacharya, S. K., & Yoshimura, K. (2016). Controlling factors of rainwater and water vapor isotopes at Bangalore, India: Constraints from observations in 2013 Indian monsoon. *Journal of Geophysical Research: Atmospheres*, *121*(23). https://doi.org/10.1002/2016JD025352

Ramos, R. D., LeGrande, A. N., Griffiths, M. L., Elsaesser, G. S., Litchmore, D. T., Tierney, J. E., et al. (2022). Constraining clouds and convective parameterizations in a climate model using paleoclimate data. *Journal of Advances in Modeling Earth Systems*, *14*(8), e2021MS002893. https://doi.org/10.1029/2021MS002893

Risi, C., Bony, S., Vimeux, F., Chong, M., & Descroix, L. (2010). Evolution of the stable water isotopic composition of the rain sampled along Sahelian squall lines. *Quarterly Journal of the Royal Meteorological Society*, *136*(S1), 227–242. https://doi.org/10.1002/qj.485

Rozanski, K., Araguás-Araguás, L., & Gonfiantini, R. (1993). Isotopic patterns in modern global precipitation. In *Climate change in continental isotopic records* (pp. 1–36). American Geophysical Union. https://doi.org/10.1029/GM078p0001

Samuels-Crow, K. E., Galewsky, J., Sharp, Z. D., & Dennis, K. J. (2014). Deuterium excess in subtropical free troposphere water vapor: Continuous measurements from the Chajnantor Plateau, northern Chile. *Geophysical Research Letters*, *41*(23), 8652–8659. https://doi.org/10.1002/2014GL062302

Schotterer, U., Oldfield, F., & Froehlich, K. (1996). GNIP global network for isotopes in precipitation. Laederach AG. http://inis.iaea.org/search/search.aspx?orig_q=RN:30013279

Sinha, N., & Chakraborty, S. (2020). Isotopic interaction and source moisture control on the isotopic composition of rainfall over the Bay of Bengal. *Atmospheric Research*, *235*, 104760. https://doi.org/10.1016/j.atmosres.2019.104760

Tian, L., Yu, W., Schuster, P. F., Wen, R., Cai, Z., Wang, D., et al. (2020). Control of seasonal water vapor isotope variations at Lhasa, southern Tibetan Plateau. *Journal of Hydrology*, *580*, 124237. https://doi.org/10.1016/j.jhydrol.2019.124237

Vimeux, F., & Risi, C. (2021). Isotopic equilibrium between raindrops and water vapor during the onset and the termination of the 2005–2006 wet season in the Bolivian Andes. *Journal of Hydrology*, *598*, 126472. https://doi.org/10.1016/j.jhydrol.2021.126472

Vimeux, F., Tremoy, G., Risi, C., & Gallaire, R. (2011). A strong control of the South American SeeSaw on the intra-seasonal variability of the isotopic composition of precipitation in the Bolivian Andes. *Earth and Planetary Science Letters*, *307*(1), 47–58. https://doi.org/10.1016/j.epsl.2011.04.031

Wang, X., Edwards, R. L., Auler, A. S., Cheng, H., Kong, X., Wang, Y., et al. (2017). Hydroclimate changes across the Amazon lowlands over the past 45,000 years. *Nature*, *541*(7636), 204–207. https://doi.org/10.1038/nature20787

Wei, Z., Lee, X., Aemisegger, F., Benetti, M., Berkelhammer, M., Casado, M., et al. (2019). A global database of water vapor isotopes measured with high temporal resolution infrared laser spectroscopy. *Scientific Data*, *6*(1), 180302. https://doi.org/10.1038/sdata.2018.302

Wong, M. L., Wang, X., Latrubesse, E. M., He, S., & Bayer, M. (2021). Variations in the South Atlantic Convergence Zone over the mid-to-late Holocene inferred from speleothem $d^{18}O$ in central Brazil. *Quaternary Science Reviews*, *10*. https://doi.org/10.1016/j.quascirev.2021.107178

Yu, W., Tian, L., Ma, Y., Xu, B., & Qu, D. (2015). Simultaneous monitoring of stable oxygen isotope composition in water vapour and precipitation over the central Tibetan Plateau. *Atmospheric Chemistry and Physics*, *15*(18), 10251–10262. https://doi.org/10.5194/acp-15-10251-2015

Zwart, C., Munksgaard, N. C., Kurita, N., & Bird, M. I. (2016). Stable isotopic signature of Australian monsoon controlled by regional convection. *Quaternary Science Reviews*, *151*(Supplement C), 228–235. https://doi.org/10.1016/j.quascirev.2016.09.010